

High-sensitivity methanol gas sensor based on rare earth (Er, Tm and Ho) doping In₂O₃ material

Yuhong Zhang, Wenlong Kang, Bing Liu, and Hang Liu*

School of electrical and computer engineering, Jilin jianzhu university, Changchun 130118, China

*E-mail: liuhang76@163.com

Received: 7 October 2022 / Accepted: 23 November 2022 / Published: 27 December 2022

In this paper, the pure and rare earth (RE=Er, Tm and Ho) doped In₂O₃ materials have been synthesized with facile solvothermal method. The obtained powder samples were coated as sensing film on ceramic tube for fabricating methanol sensor. The gas-sensing performance of gas sensors were investigated in detail. The gas response was enhanced and the optimum operating temperature was decreased for RE doped In₂O₃ materials. Among them, the Er/In₂O₃ sample shown the better gas sensing properties, and the gas sensitivity has reached two times higher than that of the pure In₂O₃ for 50 ppm methanol. The enhanced sensor response of the fabricated sensor has been ascribed to the increased surface basicity and lattice defects. Moreover, Er-doped In₂O₃ sensor has exhibited super fast response time(2 s), good repeatability and selectivity. The enhancement of gas sensing performances could be attributed to a combination of the increased surface basicity and lattice defects.

Keywords: Rare earth; methanol sensor; enhancement; basicity;

1. INTRODUCTION

As a typical clean liquid fuel and organic solvent, methanol is extensively used in industrial field. However, the methanol can attack on the human nervous system, which causes headaches, giddiness, blindness and even death. Once the people are exposed to 200 ppm methanol, the obvious damage will occur [1, 2]. Therefore, the accurate detection for methanol has become a significant topic. It is urgent to design a convenient and stable sensor for monitoring methanol in the atmosphere. In recent years, some different methods have been used to detect methanol, such as spectrophotometry, chromatography and electrochemical analysis[3]. Among them, the spectrophotometry and chromatography have high-accuracy but they have larger volume, higher price and complex analysis process, which limit the development of them in practical. While the chemical gas sensors based on the metal oxide semiconductor(MOS) have excellent performance with higher

sensitivity, strong operability and lower power, due to their significant intrinsic performance (larger specific surface area and higher surface adsorption) [4].

The metal-oxide semiconductors, including indium oxide (In_2O_3), tin oxide (SnO_2), ferric oxide (Fe_2O_3), zinc oxide (ZnO), titanium dioxide (TiO_2), etc. have been extensively applied to resistive-type gas sensors [5, 6]. For example, Sinha et al. [7] have demonstrated that the ZnO microrods show significant gas sensing performance with the ultra-high sensitivity of 4.41×10^4 % for 100 ppm methanol at 300 °C [gas sensitivity, $S_g = (I_g - I_a) / I_a \times 100\%$]. The ultra-fast response (200 ms) and recovery (120 ms) times have been obtained at 300 °C, respectively. Qian et al. [8] design the methanol gas sensors based on silver-doped LaFeO_3 molecularly. The sensor response also is measured for 5 ppm methanol at 195 °C and 215 °C. Chen et al. [9] investigate the methanol sensing performances of the 5 wt% La doped SnO_2 nanomaterials, the response for 75 ppm methanol reaches 29.5 at the optimal working temperature of 220 °C [sensor response, $S = R_a / R_g$]. Although some methanol sensors have been reported, but the development of the low detection limit and higher sensitivity methanol sensor still is the major research direction.

The In_2O_3 is an n-type semiconductor with high conductivity and a broad band gap between 3.55 and 3.75 eV, that has become a potential contender material in the practice of gas sensor [10, 11]. The different morphologies' In_2O_3 materials, such as nanofilms [12], nanotubes [13], nanofibers [14], nanospheres [15], have been prepared through physical and chemical methods. It is well known that the surface active sites, surface-to-volume ratio, band structure, the gas penetration and diffusion are all affected by the morphology of sensing materials, that is a key component for improving gas sensor property [16, 17]. Chavan et al. [12] have explored the synthesis of nano-Ag/ In_2O_3 and pure In_2O_3 thick films through standard screen-printing technique and found that the Ag addition could contribute to increase the ethanol sensing properties. Ma et al. [18] have obtained n-ZnO/n- In_2O_3 heterojunction for methanol detection and the fast response/recovery time of 100 ppm methanol is about 6/7 s, respectively. Sun et al. [19] have synthesized porous single-crystal In_2O_3 nanosheet as NO_x gas sensors, which present a ppb levels detection limit and high response (89.48) to 97 ppm NO_x . Besides, the doping with unique elements is another useful approach to increase the gas sensing behavior. Recently, the RE elements as dopant ions have attracted great attention because of their peculiar resistor, magnetic, electrochemical and optical properties. Anand et al. [20] have reported that the 10% Dy-doped In_2O_3 sensor showed the highest response for 50 ppm ethanol at 300 °C and 50 ppm of acetone at 350 °C. Mohanapriya et al. [21] have synthesized 6 mol% Ce-doped SnO_2 hollow nanofibers, the materials exhibit the response of 265 toward 50 ppm ethanol at 250 °C. Kasirajan et al. [22] report that the ZnO:RE (Gd, Nd, and Sm) thin film can enhance the sensing behavior for ammonia at room temperature. Zahmouli et al. [23] have fabricated 3 at.% Gd-doped $\gamma\text{-Fe}_2\text{O}_3$ sensors. The response to 20 ppm acetone reaches 31.2 at 200 °C. From the above reports, the codoping RE ions should enhance the gas sensing response of the metal oxide semiconductor materials. To the best of our knowledge, the research about methanol gas sensors based on RE doped In_2O_3 has scarcely been mentioned.

In this paper, the pure In_2O_3 and RE doped In_2O_3 materials have been prepared with facile solvothermal process. The structural and morphological characteristics of materials have been characterized. The sensing performance and response mechanism of the sensors also have been

discussed for detecting the methanol gas. Herein, we found that Er-doped In_2O_3 material exhibited higher response and selectivity, and faster response/recover time for methanol measurement. The basic mechanism of gas sensing for RE/ In_2O_3 materials was deliberated. The results proved that the Er- In_2O_3 would be a suitable option for the methanol detector.

2. EXPERIMENTAL

2.1. Preparation of the pure and RE codoping In_2O_3

Micrometer powders of In_2O_3 doped with Er^{3+} , Tm^{3+} and Ho^{3+} were prepared by the typical solvothermal method. $\text{In}(\text{NO}_3)_3 \cdot 4.5\text{H}_2\text{O}$, $\text{Er}(\text{NO}_3)_3 \cdot 5\text{H}_2\text{O}$, $\text{Tm}(\text{NO}_3)_3 \cdot 5\text{H}_2\text{O}$ and $\text{Ho}(\text{NO}_3)_3 \cdot 5\text{H}_2\text{O}$ were used as the starting materials. All of the chemical compounds were all analytical reagent grade. Firstly, 0.14 g of $\text{In}(\text{NO}_3)_3 \cdot 4.5\text{H}_2\text{O}$, 0.14 g of sodium dodecyl sulfate (SDS) and 1.00 g of urea were dissolved in a mixture of 10 mL anhydrous ethanol and 30 mL deionized water with vigorous magnetically. Secondly, the mixture was moved to a Teflon-lined autoclave (50 mL), locked tightly, and retained at 120 °C for 11 h. Thirdly, the autoclave was gradually cooled in surrounding air, the resultant precipitate were fully washed with deionizer water and ethanol for two times under centrifugation, and dried for 10 h. Finally, the as-obtained white powder was calcined at 500 °C for 2 h in muffle furnace at a broiling rate of 2 °C/min to produce In_2O_3 material. Similarly, three In_2O_3 materials individually doped with Er, Tm, and Ho were prepared by adding 1.0 mol% of each $\text{Er}(\text{NO}_3)_3 \cdot 5\text{H}_2\text{O}$, $\text{Tm}(\text{NO}_3)_3 \cdot 5\text{H}_2\text{O}$ and $\text{Ho}(\text{NO}_3)_3 \cdot 5\text{H}_2\text{O}$ separately to the solution of $\text{In}(\text{NO}_3)_3 \cdot 4.5\text{H}_2\text{O}$. The same process is used as the above description for preparing pure In_2O_3 materials.

2.2. Characterization and Sensor measurement

The crystal structures of all samples were employed by X-ray diffraction (XRD, RIGAKU Ultima IV) with $\text{Cu K}\alpha 1$ radiation ($\lambda = 0.15406$ nm). The morphology of sample was observed by using FE-SEM(Quanta 450). Transmission electron microscopy (TEM) images were recorded on FEI Tecnai G2 F20 microscope operated at 200 kV. The inductively coupled plasma optical emission spectrometer(ICP-OES, Agilent 725) was used to evaluate the concentration of the Er, Tm and Ho ion in the In_2O_3 samples.

For investigating the gas sensing performances of all samples, the resistance sensor was fabricated and the structure was shown in Fig.1(a)(b). The ceramic tube with a Ni-Cr wire coil was applied to prepare gas sensor, and it was welded on substrate. First, the about 2 mg as-synthesized samples were hybridized with a proper ratio of deionized water to form a size. Then, the size was subsequently coated with fine brush onto an tube (0.8 mm in internal diameter, 1.2 mm in external diameter, 4 mm in length equipped with a pair of Au electrodes) to construct a sensing film of thickness around 40 μm . At last the obtaining sensing devices were calcined at 400 °C for 2 hours after drying in the air for 20 minutes. A CGS-8 system (Beijing Elite Tech Co. Ltd., China) was utilized to provide current for the sensor and listed the data in every moment. For a common n-type

semiconductor In_2O_3 , the sensor response (γ) to oxidizing and reducing gas were defined as $\gamma = R_{\text{gas}}/R_{\text{air}}$ and $\gamma = R_{\text{air}}/R_{\text{gas}}$, where R_{air} denotes the resistance of sensor in the air and R_{gas} denotes the resistance of sensor in the test gas. Besides that, the response (t_{res}) and recovery time (t_{rec}) were calculated using the time it took to achieve a 90 % overall resistance value change.

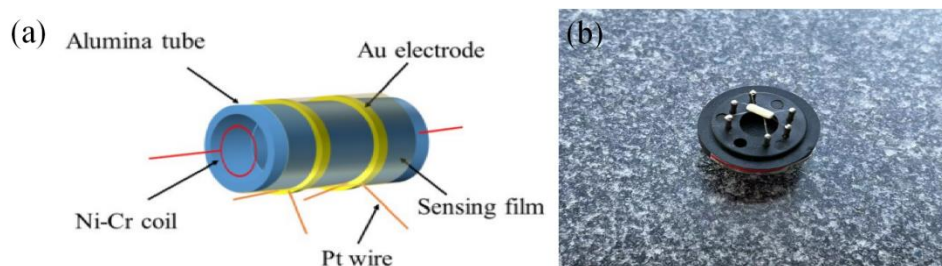


Figure 1. Schematic illustrations:(a) the structure diagram of gas sensor configuration,(b) the prepared gas sensor

3. RESULTS AND DISCUSSION

3.1. Structural and morphological characteristics

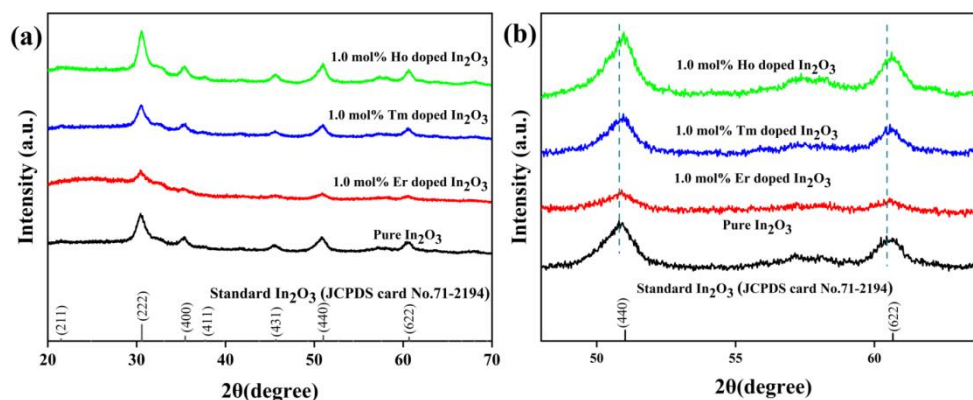


Figure 2(a) X-ray diffraction patterns of pure In_2O_3 and $\text{In}_2\text{O}_3:\text{Er}$, $\text{In}_2\text{O}_3:\text{Tm}$, $\text{In}_2\text{O}_3:\text{Ho}$ particles, (b) Comparison of (440) and (622) peaks laction from X-ray diffraction patterns for pure In_2O_3 and $\text{In}_2\text{O}_3:\text{Er}$, $\text{In}_2\text{O}_3:\text{Tm}$, $\text{In}_2\text{O}_3:\text{Ho}$ samples.

To explore the crystal phases of RE (Er, Tm and Ho) doped In_2O_3 and pure In_2O_3 samples, the XRD patterns of the samples are measured. As shown in Fig. 1(a), the diffraction peaks of all the samples are in good agreement with the cubic phase of In_2O_3 (JCPDS card No.71-2194). Owing to the lower RE ions incorporations, the additional peaks matching to dopants have not been detected in Fig. 1(a). The valence and coordination number of Er^{3+} , Tm^{3+} and Ho^{3+} ions are similar to that of In^{3+} ions in RE^{3+} doped In_2O_3 system. So the location of In^{3+} ions can be occupied by Er^{3+} , Tm^{3+} and Ho^{3+} ions. For the further research of the effects of rare earth (Er^{3+} , Tm^{3+} and Ho^{3+}) on the phase, the (440) and (622) diffraction peaks were amplified to analyze the difference between them (shown in Fig. 2(b)).

Through comparing the peaks of Er^{3+} , Tm^{3+} and Ho^{3+} -doped In_2O_3 to that of pure In_2O_3 , the (440) and (622) diffraction peaks of RE doped samples have small angle shift to higher 2θ values for RE doped In_2O_3 (Fig. 4(b)), demonstrating that the crystal structure deformation of In_2O_3 caused by rare earth dopants. The difference of ionic radius generates the change of crystal lattice of In_2O_3 . Because the radius of RE(Er^{3+} (0.88 Å), Tm^{3+} (0.87Å), Ho^{3+} (0.901 Å))are larger than that of In^{3+} (0.80 Å), the incorporation of the RE^{3+} ions will bring about a increase of the lattice parameter, and eventually result in the large lattice deformation. Based on Debye–Scherrer formula, the lattice constant will increase when In^{3+} sites are substituted by the RE ions. Based on the XRD analysis, it demonstrates that RE^{3+} ions uniformly replace In^{3+} sites [24, 25].

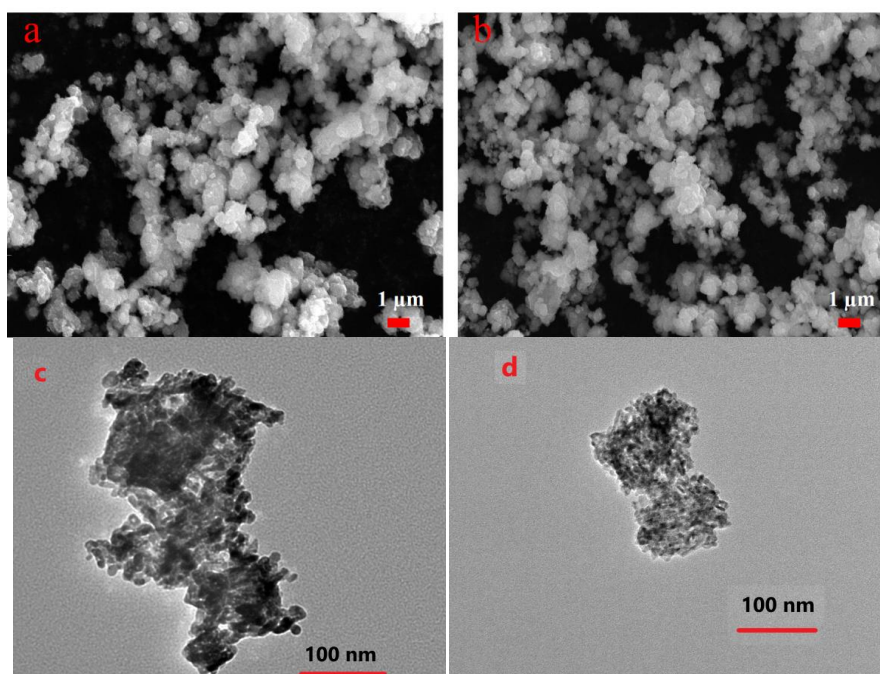


Figure 3 FESEM micrographs of (a) pure In_2O_3 , (b) 1.0 mol% Er-doped In_2O_3 . TEM micrographs of (c) pure In_2O_3 , (d) 1.0 mol% Er-doped In_2O_3

The SEM images of pure In_2O_3 and 1.0 mol%Er: In_2O_3 samples are provided in Fig.3 (a-b), the micron scales aggregates are present in all of the samples, which are composed by some nanoparticles. There is no remarkable change of morphology for two samples, which may result from two reasons: 1) These elements(Er^{3+} , Tm^{3+} , Ho^{3+} , In^{3+}) possess comparable ionic radius, so the In^{3+} is replaced with RE^{3+} ions and the crystal structure of In_2O_3 is not changed. 2) The low concentration of rare earth dopants may not remarkable change the morphology of In_2O_3 . In addition, the aggregate phenomenon should be induced by the second calcination at 500 °C in muffle furnace. The microstructure of pure In_2O_3 and 1.0 mol%Er: In_2O_3 samples are shown with TEM images in Fig.3(c) and (d). One irregular nanocrystal particles are obviously observed with the length of about 300 nm and the breadth of about 150 nm for pure In_2O_3 . With the incorporation of Er^{3+} ions, the morphology of nanoparticles is broken a little, and scale of the particle decreases with the length of about 200 nm and the breadth of about

120 nm for 1.0 mol%Er:In₂O₃. It is very important to discuss the influence of the Er³⁺ doping on the gas sensing performance.

The doping concentration of the Er, Ho and Tm is analyzed by ICP-OES, and the results were shown in Table 1. It is obvious that the observed concentration of the Er³⁺, Ho³⁺ and Tm³⁺ ion has nearly the same quantity about 0.55 mol%. So it is suitable for the further studies. In addition, to describe consistency in the paper, the origin concentration(1 mol%) still is used in the following paragraphs.

Table 1. The RE ion additional concentrations in In₂O₃ host

Doping element	Er ³⁺	Ho ³⁺	Tm ³⁺
Concentration	0.58 mol%	0.62 mol%	0.53 mol%

3.2. Gas-sensing properties

For gas sensors, the optimal operating temperature is a critical functional characteristic. The optimal operating temperature of pure In₂O₃ and RE³⁺-In₂O₃ materials are measured to 50 ppm methanol. The relationship for both working temperatures and gas sensor responses are shown in Fig. 4. Among them, the maximum responses of Er³⁺ and Ho³⁺-doped In₂O₃ methanol sensors are obtained at the functioning temperature of 320 °C, while Tm³⁺-doped In₂O₃ and pure In₂O₃ sensors exhibit their maximum response at 300 and 340 °C, respectively. For Er³⁺-doped In₂O₃ materials, the maximum response reaches 15.67 at the optimal operating temperature 320 °C, which is higher than that of others. In addition, the responses of Er³⁺, Ho³⁺ and Tm³⁺ doped In₂O₃ materials all are increased in comparison with the pure In₂O₃. Especially, the gas response of the Er³⁺-doped In₂O₃ sample is significantly enhanced. The gas response mechanism of the RE/In₂O₃ materials will be discussed based on the grain size, oxygen adsorption and lattice distortion.

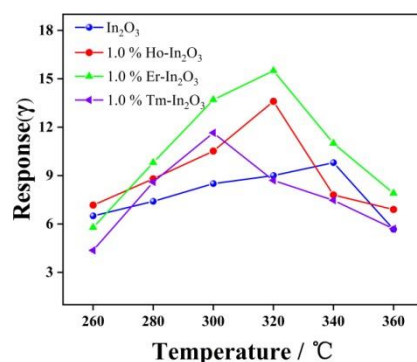


Figure 4 Response of sensors based on pur In₂O₃, In₂O₃:1 mol%Er, In₂O₃:1 mol%Ho and In₂O₃:1 mol%Tm for 50 ppm methanol at different operating temperatures.

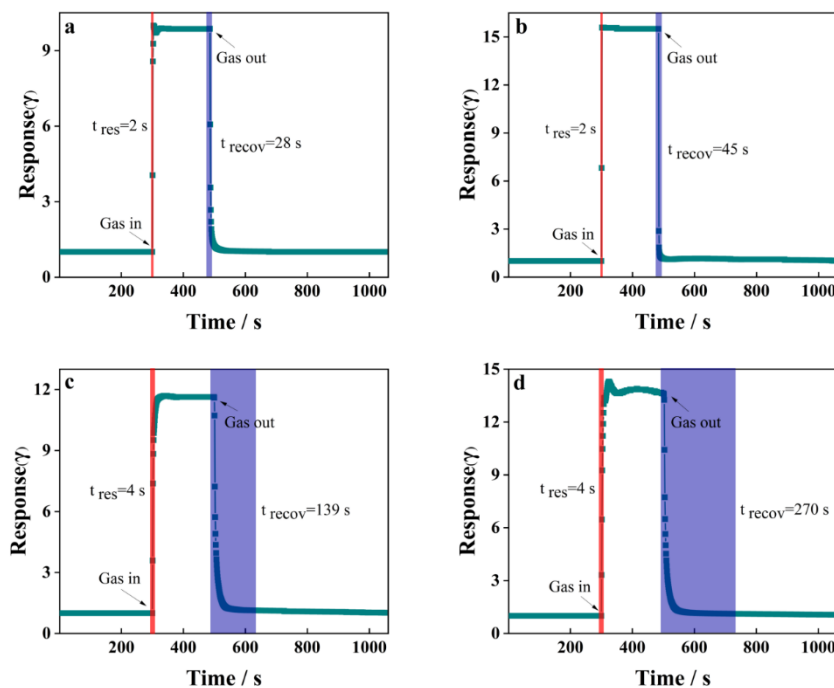


Figure 5. Typical response-recovery time of (a) In_2O_3 , (b) $\text{In}_2\text{O}_3:1 \text{ mol\%Er}$, (c) $\text{In}_2\text{O}_3:1 \text{ mol\%Tm}$, (d) $\text{In}_2\text{O}_3:1 \text{ mol\%Ho}$ samples to 50 ppm methanol vapor at the optimal operating temperature.

The best sensitivity of $\text{Er}^{3+}/\text{In}_2\text{O}_3$ owes to its larger lattice distortion and higher surface activity, which bring about largest interaction between methanol molecules and adsorbed oxygen. According to the previous report, the basicity nature of the Ho, Er and Tm elements follows the sequence ($\text{Er} > \text{Ho} > \text{Tm}$) [26]. Based on this point of view, the different gas-sensing performance of Er-doped In_2O_3 material and that of Ho-doped In_2O_3 , Tm-doped In_2O_3 , as well as pure In_2O_3 material may also link to their different basicity. So the Er-doped In_2O_3 sensor shows the strongest response to methanol.

For the application of the gas sensor, the response/recovery times are also important parameters. Fig. 5 presents the transient relative response of pure In_2O_3 and RE (Er, Tm and Ho) doped In_2O_3 sensors with methanol concentration 50 ppm at their own operating temperature. All the samples show the super fast response time. The response times of the four samples are 2, 2, 4 and 4 s, respectively. The recovery times of pure In_2O_3 (28 s) and $\text{Er}/\text{In}_2\text{O}_3$ (45 s) are faster than that of $\text{Tm}/\text{In}_2\text{O}_3$ (139 s) and $\text{Ho}/\text{In}_2\text{O}_3$ (270 s) samples. Obviously, the Er doping In_2O_3 materials show the best gas response and faster response/recovery times for methanol detection. So the methanol sensing performances of $\text{Er}/\text{In}_2\text{O}_3$ sample are further investigated in detail.

The dynamic response curves of $\text{In}_2\text{O}_3:1 \text{ mol\%Er}^{3+}$ sensor for different concentration methanol are presented in Fig. 6(a). The gas responses are increased with the enhancement of the methanol concentration. Specifically, the sensor responses are approximately 3.57, 11.91, 15.67, 19.68, and 22.40 toward 10, 30, 50, 70, and 100 ppm methanol, respectively.

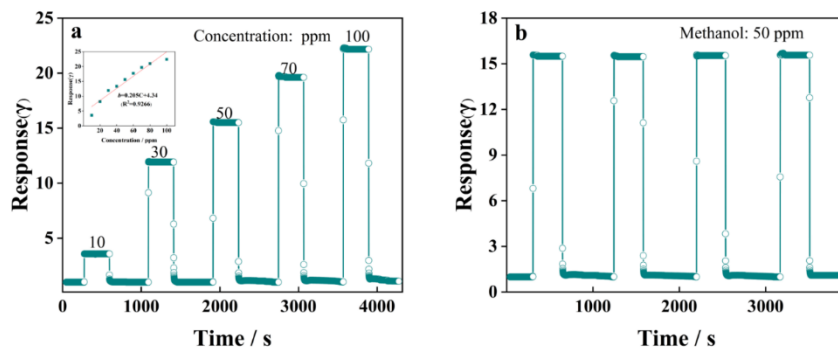


Figure 6. (a) Dynamic response curves of 1.0 mol% Er doped In_2O_3 sensor to different concentrations of methanol at 320 °C; (b) Repeatability curve of the sensor towards 50 ppm methanol at 320 °C.

Notably, the linear relationship between response value (γ) and methanol concentration (C) ranging from 10 to 100 ppm can be described as $\gamma = 0.205C + 4.34$ with a coefficient of $R^2 = 0.9266$ (shown in the inset of Fig. 6a). Additionally, the stability of the methanol gas sensor is also confirmed. Four reversible cycles of the dynamic response curve (Fig. 6b) keep its initial response value without clear floating, demonstrating its good reproducibility and stability of the 1 mol% Er-doped In_2O_3 sensor.

Another important parameter for gas sensor is the selectivity, which is the ability of a sensor to identify potentially disturbing gases. Therefore, the responses of Er-doped In_2O_3 and pure In_2O_3 sensors toward 50 ppm xylene, SO_2 , NO_2 , ammonia, and toluene are measured at 320 °C. From Fig. 7, the response of the Er/ In_2O_3 sensor to 50 ppm methanol is about 15.2, which is at least two times more than other test gases.

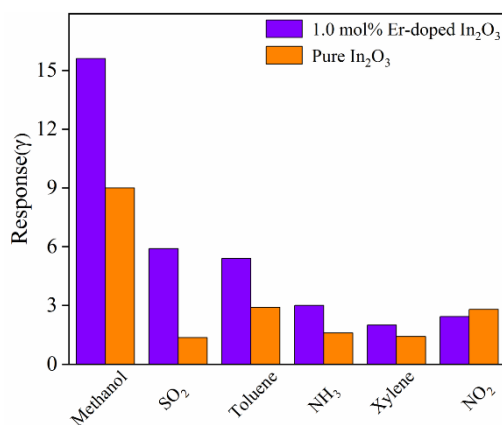


Figure 7. Response of pure and 1.0 mol% Er-doped In_2O_3 to 50 ppm of various test gases at 320 °C.

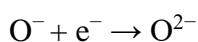
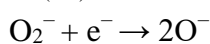
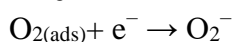
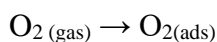
A comparison of reported methanol sensors is illustrated in Table 2. It can be found that the Er doped In_2O_3 materials shown the faster response/recovery time and higher methanol response than those reported materials.

Table 2. Sensing performance of different materials to methanol gas

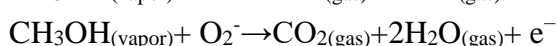
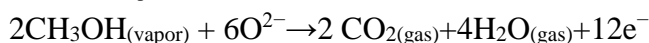
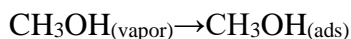
Sensing materials	Optimal temperature °C	concentration	Sensitivity	value/recovery time (s)	Ref.
Honeycomb-like SnO ₂	320	50 ppm	R _a /R _g = 7.7	10/9	[27]
Au-decorated ZnO	300	50 ppm	R _a /R _g = 7	-/-	[28]
ZnO/SnO ₂ hierarchical architectures	300	100 ppm	R _a /R _g = 9.6	~/10	[29]
Al-doped ZnO thin films	270	500 ppm	(R _g -R _a)/R _a =0.12	~/380	[30]
α-Fe ₂ O ₃ polyhedral crystals	340	50 ppm	R _a /R _g =2.5	-/-	[31]
ZnO hollow microsphere	400	200 ppm	R _a /R _g =9.6	-/-	[32]
WO ₃ particles	260	100 ppm	R _a /R _g =24	19/8	[33]
Fe ₂ O ₃ discoid crystal	250	100 ppm	R _a /R _g =6.4	-/-	[34]
Pd _{0.5} Pd ₃ O ₄ -load ZnO	260	50 ppm	R _a /R _g =10.5	1/5	[35]
Er-doped In ₂ O ₃ material	320	50 ppm	R _a /R _g =15.67	2/45	This work

3.3. Gas response mechanism

The possible gas response process of RE doped In₂O₃ materials may be clarified with the surface-resistance-controlled model. It is well known, the In₂O₃ belongs to n-type semiconductor in which free electrons are prime carriers. The general response mechanism contributes to the interaction between target gas and adsorbed oxygen (O₂⁻, O₂²⁻ and O⁻) on sensing material surfaces, resulting in the electrical conductance change of the In₂O₃ sensor[36]. As shown in Fig. 8, once the In₂O₃ is placed to air, it will produce the formation of an electron depletion layer and an increased resistance. The possible reactions can be clarified as follows:



Upon exposing the sensing materials to methanol, the chemisorbed oxygen generates reaction with methanol molecules and the accepted electrons will return to the In₂O₃, which brings about the decreasing for both the thickness of the electron depletion layer and the sensor resistance[37].



As a result, the response ($\gamma = R_{\text{air}}/R_{\text{gas}}$) will increase in reducing gas (such as methanol, toluene, NH₃ and xylene). The unusual gas sensing performance of Er-In₂O₃ sensor may attributed to the following reasons. Firstly, the In³⁺ and Er³⁺ have a comparable ionic radius, In³⁺ sites will be substituted by Er³⁺ ions after Er³⁺ doping into In₂O₃, which generates the lattice defects of In₂O₃. The increase of the lattice defects will contribute to the enhancement of the gas adsorption on the material

surface[38, 39]. As a result, the gas sensing performance can be greatly improved. Secondly, the basic characteristic of RE oxide benefits sensing reaction because of the surface basicity of Er^{3+} -doped In_2O_3 thereby enhances sensor response.

In addition, when the In_2O_3 materials are exposed to oxidizing gas(such as NO_2 and SO_2), the oxidizing gas molecules will capture electrons from the conductance band and react with the absorbed oxygen species, resulting in the concentration decrease of the free charge carries. As a result, the resistance of the sensors will increase, and the response($\gamma=R_{\text{gas}}/R_{\text{air}}$) will increase in oxidizing gas(such as SO_2 and NO_2).

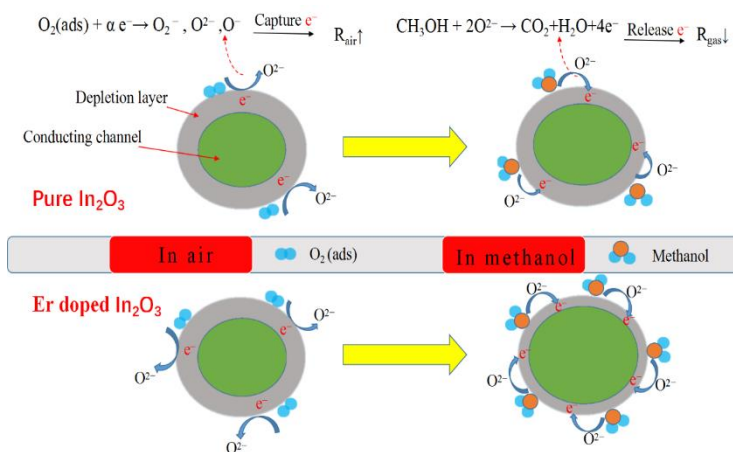


Figure 8. The schematic diagram of possible gas sensing mechanism for pure and Er-doped In_2O_3 samples.

4. CONCLUSION

In conclusion, the pure In_2O_3 and RE (Er, Tm and Ho) doped In_2O_3 particles have been successfully synthesized via facile solvothermal method. The crystal structures of as-prepared powders are employed by XRD, and all the samples are in good agreement with the cubic phase of In_2O_3 . The gas sensing performances of all the samples are investigated in detail. The experimental results indicate that the responses of Er^{3+} , Ho^{3+} and Tm^{3+} doped In_2O_3 materials all are increased in comparison with the pure In_2O_3 . The 1 mol% Er-doped In_2O_3 sensor exhibits the highest gas sensing performance than Tm^{3+} and Ho^{3+} doped In_2O_3 sensor toward 50 ppm methanol gas at 320 °C, and the sensitivity is 15.67. In addition, all the samples show the super fast response time. The response times of the four samples are 2, 2, 4 and 4 s, respectively. The recovery times of pure In_2O_3 (28 s) and Er/ In_2O_3 (45 s) are faster than that of Tm/ In_2O_3 (139 s) and Ho/ In_2O_3 (270 s) samples. So the Er doped In_2O_3 materials have shown the faster response/recovery time and higher methanol response. The excellent sensing properties of Er/ In_2O_3 materials could be attributed to a combination of the increased surface basicity and lattice defects. Consequently, it can prove that the codoping RE ions will be a prospective strategy for increasing the gas sensing properties of semiconductor.

ACKNOWLEDGMENTS

This work was supported by Natural Science Foundation of China (Grant No:61705077); Project of Jilin Provincial Science and Technology Department (20200403072SF); Project of Jilin Province Development and Reform Commission (2019C048-4, 2020C021-5).

References

1. Y. Li, D. Deng, X. Xing, C. Nan and Y. Wang, *Sensor. Actuat. B-Chem.*, 237 (2016) 133-141.
2. D. Meng, S. Zhang, T. Thomas, R. Zhao and M. Yang, *Sensor. Actuat. B-Chem.*, 308 (2020) 127713.
3. A. Patah, W. Kasim and B. Yulianto, *Key. Eng. Mat.*, 811 (2019) 113-119.
4. Z. Li, H. Li, Z. Wu, M. Wang, J. Luo, H. Torun, P. Hu, C. Yang, M. Grundmann and X. Liu, *Mater. Horiz.*, 6 (2019) 470-506.
5. H. Ji, W. Zeng and Y. Li, *Nanoscale.*, 11 (2019) 22664-22684.
6. B.Y. Wei, M.C. Hsu, P.G. Su, H.M. Lin, R.J. Wu and H.J. Lai, *Sensor. Actuat. B-Chem.*, 101 (2004) 81-89.
7. M. Sinha, R. Mahapatra, B. Mondal and R. Ghosh, *Electron. Mater.*, 46 (2017) 2476-2482.
8. Q. Rong, Y. Zhang, T. Lv, K. Shen, B. Zi, Z. Zhu, J. Zhang and Q. Liu, *Nanotechnology.*, 29 (2018) 145503.
9. Y. Chen, Z. Dong, X. Xue, S. Chen, A. Natan, Y. Lv, C. Chen, Y. Yang, W. Cen and Y. Yang, *Appl. Phys. A-Mater.*, 126 (2020) 1-10.
10. D. Wei, Z. Huang, L. Wang, X. Chuai, S. Zhang and G. Lu, *Sensor. Actuat. B-Chem.*, 255 (2018) 1211-1219.
11. Y. Zhang, C. Jia, Q. Kong, N. Fan, G. Chen, H. Guan and C. Dong, *ACS. Appl. Mater. Inter.*, (2020) 26161-26169.
12. D.N. Chavan, V.B. Gaikwad, P.K. Khanna, G.E. Patil, D.D. Kajale and G.H. Jain, *Sensors.*, 2011 (2011) 539-556.
13. J. Bai, Y. Luo, B. An, Q. Wang, X. Cheng, J. Li, X. Pan, J. Zhou, Y. Wang and E. Xie, *Sensor. Actuat. B-Chem.*, 311 (2020) 127938.
14. X.J. Zhang and G.J. Qiao, *Appl. Surf. Sci.*, 258 (2012) 6643-6647.
15. Z. Li, H.F. Fei, Y. Tan, X. Zhang, Z. Xie and Z. Zhang, *RSC. Adv.*, 5 (2015) 38093-38099.
16. P. Sun, X. Mei, Y. Cai, J. Ma, Y. Sun, X. Liang, F. Liu and G. Lu, *Sensor. Actuat. B-Chem.*, 187 (2013) 301-307.
17. Y. Li, W. Luo, N. Qin, J. Dong, J. Wei, W. Li, S. Feng, J. Chen, J. Xu and A.A. Elzatahry, *Angew. Chem.*, 126 (2014) 9181-9186.
18. L. Ma, H. Fan, H. Tian, J. Fang and X. Qian, *Sensor. Actuat. B-Chem.*, 222 (2016) 508-516.
19. S. Li, W. Fang, Y. Ying, Y. Hui and K. Shi, *RSC. Adv.*, 7 (2017) 33419-33425.
20. K. Anand, J. Kaur, R.C. Singh and R. Thangaraj, *J. Chem. Phys. Lett.*, 670 (2017) 37-45.
21. P. Mohanapriya, H. Segawa, K. Watanabe, K. Watanabe, S. Samitsu, T. Natarajan, N.V. Jaya and N. Ohashi, *Sensor. Actuat. B-Chem.*, 188 (2013) 872-878.
22. K. Kasirajan, L.B. Chandrasekar, S. Maheswari, M. Karunakaran and P.S. Sundaram, *Opt. Mater.*, 121 (2021) 111554.
23. N. Zahmouli, M. Hjjiri, S. Leonardi, L. El Mir, G. Neri, D. Iannazzo, C. Espro and M. Aida, *Mat. Sci. Semicon. Proc.*, 116 (2020) 105154.
24. T. Zhang, F. Gu, D. Han, Z. Wang and G. Guo, *Sensor. Actuat. B-Chem.*, 177 (2013) 1180-1188.
25. Z. Wang, C. Hou, Q. De, F. Gu and D. Han, *ACS. Sensors.*, 3 (2018) 468-475.
26. A.M. Maitra, *Therm. Anal. Calorim.*, 36 (1990) 657-675.
27. L. Wang, Z. Li, L. Luo, C. Zhao and L. Kang, *J. Alloy. Compd.*, 682 (2016) 170-175.
28. X. Liu, J. Zhang, L. Wang, T. Yang, X. Guo, S. Wu, and S. Wang, *J. Mater. Chem.*, 21 (2010) 349-356.

29. C. Li, X. Yin, Q. Li and T. Wang, *CrystEngComm.*, 13 (2011) 1557-1563.
30. M. Parmar and K. Rajanna, *Int. J. Smart. Sens. Int.*, 4 (2011) 710-725.
31. X. Rao, X. Su, C. Yang, J. Wang, X. Zhen and D. Ling, *CrystEngComm.*, 15 (2013) 7250-7256.
32. Y. S. Shim, H. G. Moon, D. H. Kim, L. H. Zhang, S. J. Yoon, Y. S. Yoon, C. Y. Kang and H. W. Jang, *RSC Adv.*, 3(2013)10452.
33. Z. H. Li, J. C. Li, L. L. Song, H. Q. Gong and Q. Niu, *J. Mater.Chem. A*, 1(2013)15377.
34. P. Sun, Y. W. Liu, X. W. Li, Y. F. Sun, X. S. Liang, F. M. Liu and G. Y. Lu, *RSC Adv.*, 2(2012)9824.
35. S.M. Wang, P. Wang, Z.F. Li, C.H. Xiao, B.X. Xiao, R. Zhao, T.Y. Yang and M.Z. Zhang, *RSC Adv.*, 4(2014)35375
36. X. Xu, D. Wang, W. Wang, P. Sun, J. Ma, X. Liang, Y. Sun, Y. Ma and G. Lu, *Sensor. Actuat. B-Chem.*, 171 (2012) 1066-1072.
37. Q. Zhu, Y. Zhang, J. Zhang, Z. Zhu and Q. Liu, *Sensor. Actuat. B-Chem.*, 207 (2015) 398-403.
38. C. W. Na, S.Y. Bae and J. Park, *J. Phys. Chem. B.*, 109 (2005) 12785-12790.
39. N. Singh, C. Yan and P.S. Lee, *Sensor. Actuat. B-Chem.*, 150 (2010) 19-24.

© 2022 The Authors. Published by ESG (www.electrochemsci.org). This article is an open access article distributed under the terms and conditions of the Creative Commons Attribution license (<http://creativecommons.org/licenses/by/4.0/>).